AIP | Journal of Applied Physics

Hyperbolic transmission-line metamaterials

Alyona V. Chshelokova, Polina V. Kapitanova, Alexander N. Poddubny, Dmitry S. Filonov, Alexey P. Slobozhanyuk et al.

Citation: J. Appl. Phys. **112**, 073116 (2012); doi: 10.1063/1.4758287
View online: http://dx.doi.org/10.1063/1.4758287
View Table of Contents: http://jap.aip.org/resource/1/JAPIAU/v112/i7
Published by the American Institute of Physics.

Hyperbolic transmission-line metamaterials

Alyona V. Chshelokova,[1] Polina V. Kapitanova,[1] Alexander N. Poddubny,[1,2]
Dmitry S. Filonov,[1] Alexey P. Slobozhanyuk,[1] Yuri S. Kivshar,[1,3] and Pavel A. Belov[1,4]
[1]*National Research University of Information Technologies, Mechanics and Optics (ITMO), St. Petersburg 197101, Russia*
[2]*Ioffe Physical-Technical Institute of the Russian Academy of Science, St. Petersburg 194021, Russia*
[3]*Nonlinear Physics Center, Research School of Physics and Engineering, Australian National University, Canberra ACT 0200, Australia*
[4]*Queen Mary University of London, London E1 4NS, United Kingdom*

(Received 11 July 2012; accepted 12 September 2012; published online 11 October 2012)

We demonstrate how to realize an indefinite media with hyperbolic isofrequency surfaces in wavevector space by employing two-dimensional metamaterial transmission lines. We classify different types of such media, and visualize the peculiar character of wave propagation by study of the cross-like emission pattern of a current source placed in the lattice center. Our results are supported by a solution of the Kirchhoff equations, an analytical theory, and experimental data.
 [http://dx.doi.org/10.1063/1.4758287]

Hyperbolic metamaterial, being a particular class of indefinite media, is a uniaxial system, where the transverse $\varepsilon_{xx} = \varepsilon_{yy} = \varepsilon_\perp$ and longitudinal $\varepsilon_{zz} = \varepsilon_\parallel$ dielectric constants have opposite signs.[1–3] Due to the hyperbolic isofrequency surfaces in the wavevector space, this medium exhibits a number of unusual properties. First, the waves at its boundary may exhibit negative refraction, similarly to the case of double-negative materials.[4–6] Second, the diverging density of photonic states promotes ultra-high spontaneous emission rates.[7–11] This makes a concept of hyperbolic media very promising for the broad-band tailoring of light-matter coupling and explains the ongoing intensive attempts to realize hyperbolic plasmonic metamaterials.[12] Back to 1969, Fisher and Gould were first to demonstrate experimentally the hyperbolic behavior in magnetized plasma in microwave frequency range.[13] Since then, there were studies investigating resonance cone formation, negative reflection, propagation, and focusing in a planar wire-grid network loaded with orthogonal capacitors and inductors as well as in transmission line periodic grids.[14–17]

In this paper, we aim to study the opportunity to mimic the hyperbolic metamaterials with artificial two-dimensional transmission lines. The transmission-line approach to synthesis and design of metamaterials has been developed recently.[18–23] One, two, and three-dimensional transmission-line metamaterials were introduced exhibiting both negative and positive effective material parameters. Nevertheless, artificial metamaterial transmission line with effective material parameters corresponding to hyperbolic and indefinite metamaterials have not been presented yet. Here, we extend the transmission-line approach to design and realize in experiment two-dimensional hyperbolic metamaterials. We find the relation between the material parameters of the hyperbolic medium and the values of admittances and impedances of the artificial transmission line. We design and fabricate a prototype of two-dimensional hyperbolic medium using chip capacitors and inductors mounted on a printed circuit board. We study the emission of a current source in the artificial hyperbolic medium and demonstrate experimentally the pronounced cross-like pattern.

We consider an uniaxial anisotropic hyperbolic medium characterized by the scalar permittivity ε and longitudinal and transverse permeabilities μ_{xx} and μ_{yy}. As it will be shown below, this medium can be mimicked by artificial two-dimensional transmission lines shown in Fig. 1. In particular, the dispersion equation for a TE-polarized wave, propagating in the x–y plane (magnetic field is oriented along z axis), reads

$$\frac{k_x^2}{\omega^2 \mu_{yy} \varepsilon} + \frac{k_y^2}{\omega^2 \mu_{xx} \varepsilon} = 1, \tag{1}$$

where k_x and k_y are the x and y components of the propagation vector and ω is the frequency. As is demonstrated in

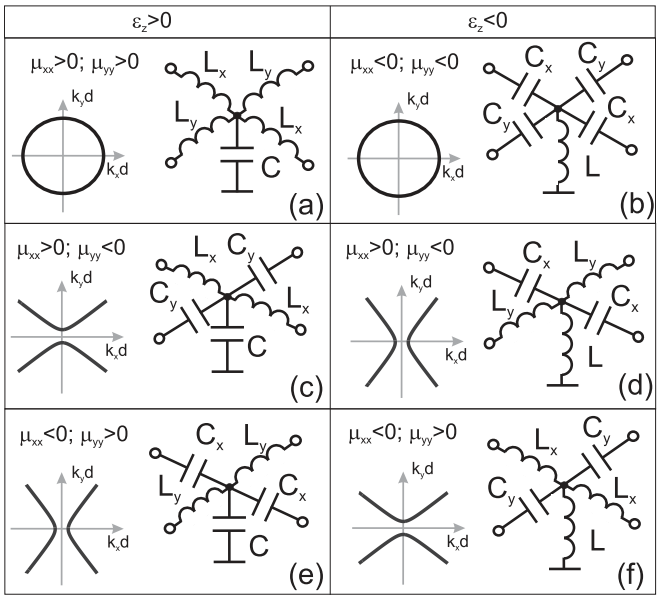

FIG. 1. Unit cells of the artificial transmission line providing elliptical and hyperbolic isofrequency curves.

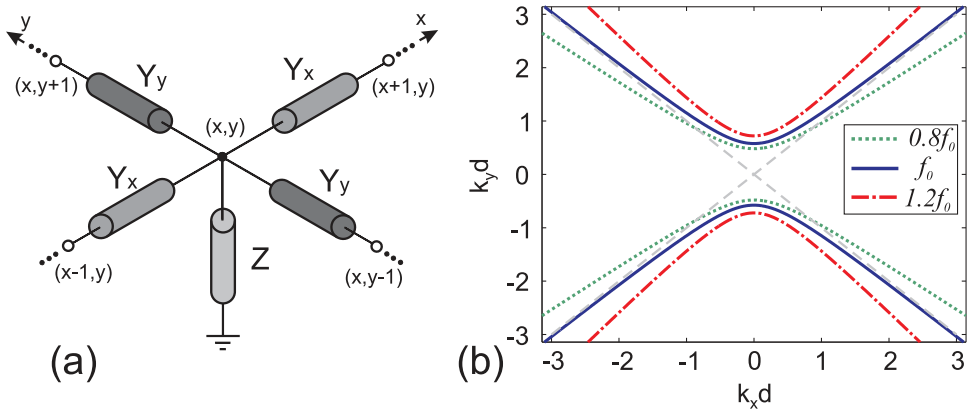

FIG. 2. (a) Unit cell of the artificial metamaterial two-dimensional transmission line structure. (b) Isofrequency curves obtained by numerical solution of the dispersion relation (4) for different frequencies. The results are obtained for the following parameters: $f_0 = 50$ MHz, $C_y = 3.2$ nF, $L_x = 3.2$ nH, and $L = 9.5$ nH.

Fig. 1, the shape of the isofrequency contour (elliptic or hyperbolic) depends on the sign of ε, μ_{xx}, and μ_{yy}.

To mimic the proposed hyperbolic medium, we consider the transmission-line metamaterial composed of the unit cells schematically shown in Fig. 2(a). For the sake of generality, the loads are represented as series admittances Y_x and Y_y and shunt impedance Z. First, we derive the dispersion equation for a two-dimensional structure consisting of infinite number of the unit cells. It can be done by summing up all the currents flowing to the node (x, y) and equating this sum to the ground current (via impedance Z). The result is

$$Y_x(U_{x-1,y} + U_{x+1,y}) + Y_y(U_{x,y-1} + U_{x,y+1}) - 2U_{x,y}(Y_x + Y_y) = U_{x,y}/Z. \quad (2)$$

In the periodic structure, we can look for a Bloch solution of the form $U_{x,y} = U_0 \exp[j(k_x d + k_y d)]$ and transform Eq. (2) to

$$Y_x \sin^2(k_x d/2) + Y_y \sin^2(k_y d/2) = -1/(4Z). \quad (3)$$

At the frequencies where the delays per unit cell are small $(k_x d \ll 1, k_y d \ll 1)$, the dispersion relation (3) can be further reduced to

$$-Y_x Z(k_x d)^2 - Y_y Z(k_y d)^2 = 1. \quad (4)$$

From comparison of Eqs. (1) and (4), one may conclude that

$$\frac{Y_x}{Y_y} = \frac{\mu_{xx}}{\mu_{yy}}, \quad (5)$$

so the series admittances Y_x and Y_y should have opposite signs to provide the hyperbolic shape of the dispersion curve. This can be realized by choosing admittances Y_x as inductances and Y_y as capacitances, or vice versa. The clear correspondence between the dispersion equations for transmission-line metamaterial and for anisotropic medium, Eqs. (1) and (4), is demonstrated by Fig. 1.

Another essential condition to mimic the hyperbolic medium is the possibility to reproduce the interference pattern of the emitted waves. The characteristic wavelength of the waves $2\pi/k$ should be on one hand larger than the unit cell size d, and on the other hand, smaller than the structure dimensions Nd, where N is the number of unit cells along an axis. Estimating typical values of kd from Eq. (4) as $1/\sqrt{|YZ|}$, we find the following requirement for both admittances Y_x, Y_y and the shunt impedance Z:

$$1 \lesssim (2\pi)^2 |Y||Z| \lesssim N^2. \quad (6)$$

Equations (5) and (6) provide the basis for design of the artificial hyperbolic medium. We stress that the effective

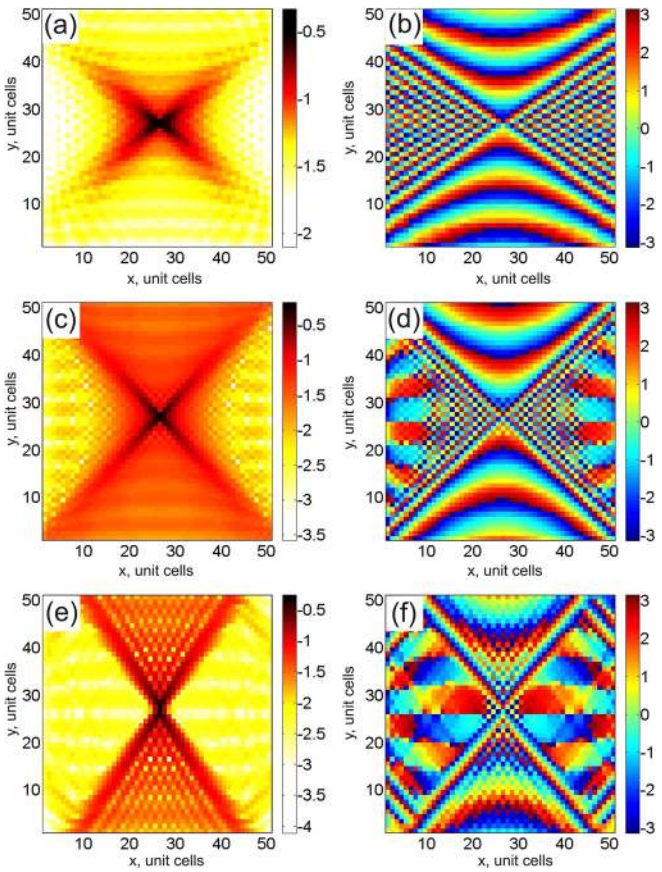

FIG. 3. Simulated voltage distribution of the two-dimensional hyperbolic medium composed of 51 × 51 unit cells. Voltage magnitude (a), (c), and (e) in logarithmic scale and phase (b), (d), and (f) for frequencies $0.8f_0$, f_0, and $1.2f_0$, respectively.

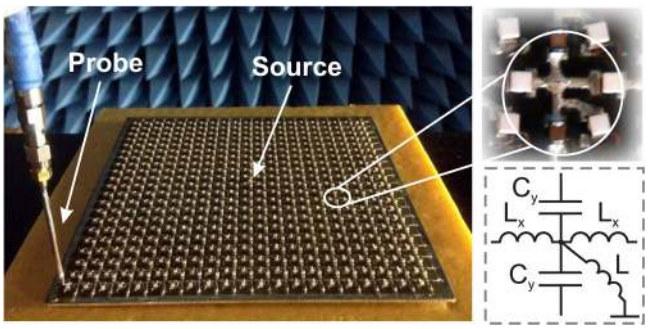

FIG. 4. Photograph of the two-dimensional hyperbolic medium prototype. The structure is composed of 21 × 21 unit cells.

medium condition Eq. (6) has not been satisfied in the previous studies: in Refs. 14 and 15 $Z = \infty$; in Refs. 16 and 17 $kd \sim \pi$ (photonic crystal regime).

In our modeling, we use the unit cell depicted in Fig. 1(f). To satisfy Eqs. (5) and (6), the values of lumped elements are chosen as $C_y = 3.2$ nF, $L_x = 3.2$ nH, and $L = 9.5$ nH assuming that $Y = j\omega C$ and $Z = j\omega L$. The operational frequency is chosen to be $f_0 = 50$ MHz to simplify the further selection of chip capacitors and inductors for fabrication of the hyperbolic medium prototype. The numerical solution of the dispersion Eq. (4) for these parameters is shown in Fig. 2(b) for different frequencies. The isofrequency curves have a hyperbolic form and the angle of the cross changes with frequency.

The peculiar properties of the hyperbolic medium are most efficiently visualized by the emission pattern of the point dipole source.[3,13] The magnitude and phase of voltage distribution excited in the structure composed of 51 × 51 unit cells is numerically found by diagonalizing Eq. (2). The results obtained for the frequencies $0.8f_0$, f_0, and $1.2f_0$ are shown in Fig. 3. The current source is placed in the structure center between the two neighboring nodes in y direction. At the edges, the structure is loaded by the resistors with $R = 1\,\Omega$ to provide the boundary matching conditions. The maximum of the voltage distribution across the medium has characteristic cross-like shape. The oscillations of the voltage phase confirm the propagation of the emitted waves in x direction and their evanescent character along y direction, in agreement with the dispersion curves shown in Fig. 2(b). We also observe a modification of the cross shape when the operational frequency changes.

The prototype of the proposed hyperbolic medium has been fabricated. The photograph of the sample composed of 21 × 21 unit cells is presented in Fig. 4. The unit cell dimension equals to $d = 9$ mm. We used commercially available chip capacitors and inductors from Murata. Accordingly to the calculated values, the following chip components were

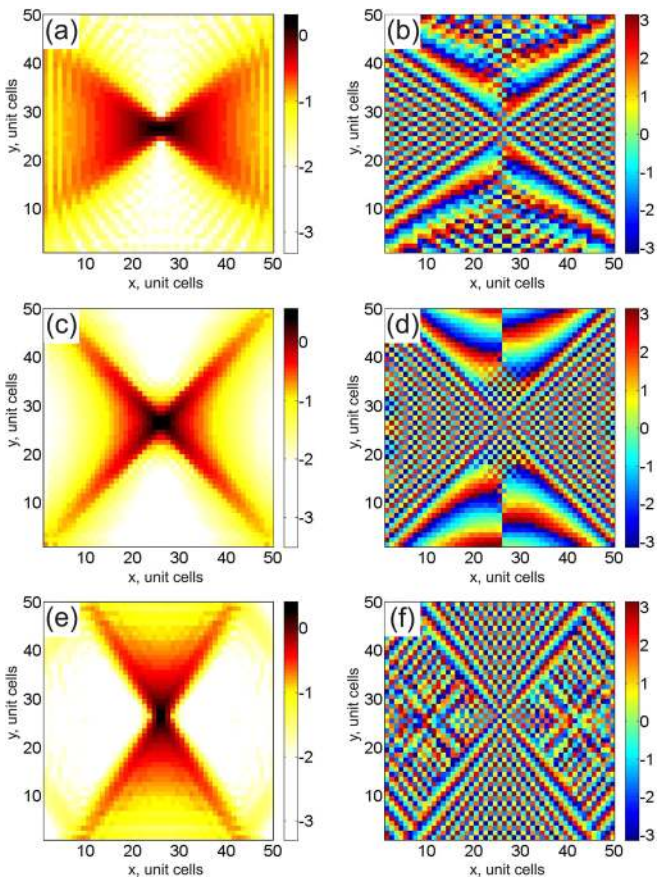

FIG. 5. Simulated current distribution of the two-dimensional hyperbolic medium composed of 51 × 51 unit cells. Current magnitude (a), (c), and (e) in logarithmic scale and phase (b), (d), and (f) for frequencies $0.8f_0$, f_0, and $1.2f_0$, respectively.

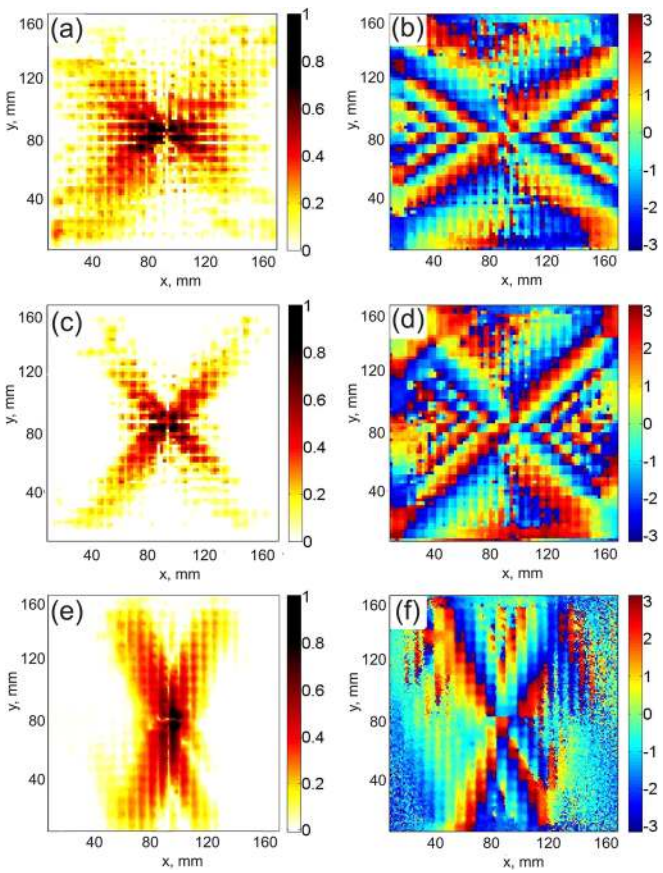

FIG. 6. Measured distribution of magnetic field: (a), (b)—magnitude and phase at 31 MHz; (c), (d)—magnitude and phase at 36 MHz; and (e), (f)—magnitude and phase at 48 MHz.

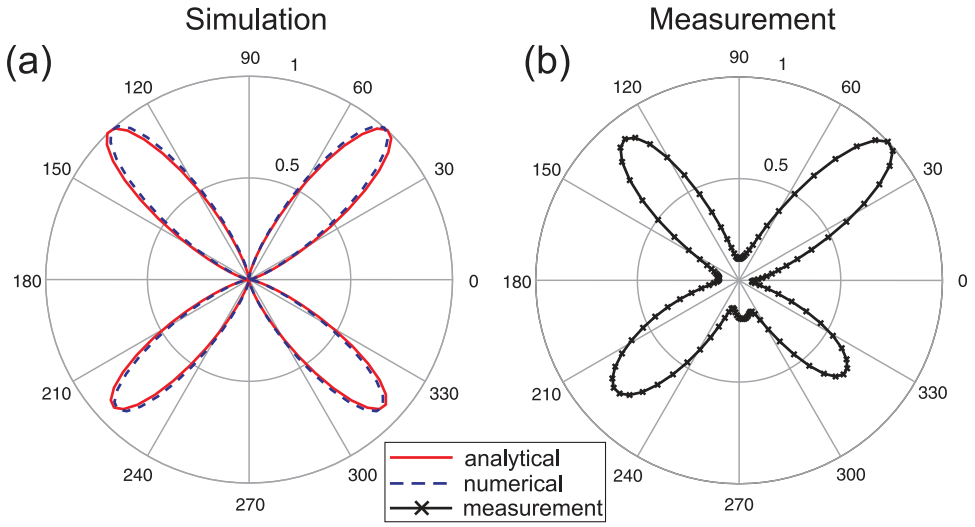

FIG. 7. Normalized angular distribution of the magnetic field.

chosen: $L_x = 3.3$ nH—inductor model LQW2BHN3N3D; $C_y = 3.3$ nF—capacitor model RM216R71H332K; and $L = 10$ nH—inductor model LQW2BHN10NJ. The components have been mounted on a FR4 dielectric substrate ($\varepsilon_r = 4.4$) with the help of a soldering robot Everprecision EP-SR. To provide the matching conditions, 1 Ω resistors (model ERJ6BQF1R0V) from Panasonic have been mounted at the edges. The prototype dimensions are 170 mm × 170 mm.

During the experimental investigation, we have measured the near field at 1 mm above the top surface of the prototype by an automatic mechanical near-field scanner. The structure was excited by a vector network analyzer (Agilent E8362C PNA) in the center. A magnetic probe[24] was used for measurements, so we can measure only the magnetic field distribution. To explain the measurement results, we have calculated the current circulation around each unit cell and we assume it should be approximately proportional to the measured magnetic field. The results of the simulated currents are shown in Fig. 5. Comparing Figs. 5 and 4, we see that the magnetic field pattern retains the cross-like shape, but the phase pattern changes as compared to that for the voltage. The phase jump in the phase portrait is observed at the vertical line $x = 25$ unit cells [Figs. 5(b) and 5(d)]. This is a specific feature of the magnetic field distribution of a discrete source. Magnetic field itself remains continuous because its amplitude vanishes at the phase jumps.

The measured magnetic field is presented in Fig. 6. The central frequency has been shifted to $f_0 = 36$ MHz due to the influence of the dielectric substrate, which was not taken into account during the simulation. In accordance with the simulation, we observe the distribution of the measured magnetic field with the shape of the cross. From the phase pictures, one can confirm the wave propagation in the y direction. The cross angle is equal to 45° at the central frequency. With the frequency decrease the angle of the cross narrows and at the frequency 31 MHz, it equals to 30°. When the frequency increases up to 48 MHz, the angle of the cross is 120°.

To analyze the obtained results in more detail, we calculate the angular distribution of the magnetic field in the "far-field" zone at the distance $\sim N/2$ from the origin, where N is the number of unit cells along x, y directions. The angular dependence corresponding to Fig. 5(c) is shown in Fig. 7(a) by the dashed curve. It is also instructive to compare the numerically simulated distribution with the effective medium theory. In this case, the magnetic field is extracted from the analytical Green function of Eq. (1) in the long–wavelength limit

$$U = \frac{d}{dy} H_0^{(1)} \left[\left(-\frac{(x-x_0)^2}{Y_x Z} - \frac{(y-y_0)^2}{Y_y Z} \right)^{1/2} \right], \qquad (7)$$

where x_0 and y_0 are the source coordinates. Equation (7) can be obtained by replacing the finite differences in Eq. (1) by the second-order derivatives and then scaling the result for the well-known isotropic case[3] $(\Delta + 1) H_0^{(1)}(\sqrt{x^2 + y^2}) = 4i\delta(x)\delta(y)$ using the transformation $x \to ix/\sqrt{Y_x Z}$, $y \to iy/\sqrt{Y_y Z}$. The derivative over y in Eq. (7) accounts for the vertical dipole source in Eq. (1): the voltage of different signs is applied to the two vertically adjacent lattice nodes. Since the reflection from the edges is weak [Fig. 5], the solution (7) for the infinite grid reproduces well the calculated angular distribution for the finite structure, see the solid curve in Fig. 7(a). The angular distribution of the measured magnetic field at the frequency 36 MHz is depicted in Fig. 7(b) and agrees with Fig. 7(a).

To summarize, we have analyzed theoretically and verified experimentally the hyperbolic media based on artificial metamaterial two-dimensional transmission lines. We have calculated the structure parameters (capacitances, inductances) and observed the pronounced cross-like emission pattern of the current source, being the fingerprint of a hyperbolic medium. We have fabricated the prototype and experimentally confirmed our theoretical results.

The authors acknowledge a support from the Ministry of Education and Science of the Russian Federation, Russian

Foundation for Basic Research, Dynasty Foundation (Russia), the Engineering and Physical Sciences Research Council (UK), and the Australian Research Council (Australia).

[1]D. R. Smith and D. Schurig, Phys. Rev. Lett. **90**, 077405 (2003).
[2]I. V. Lindell, S. A. Tretyakov, K. I. Nikoskinen, and S. Ilvonen, Microwave Opt. Technol. Lett. **31**, 129 (2001).
[3]L. Felsen and N. Marcuvitz, *Radiation and Scattering of Waves* (Wiley Interscience, New York, 2003).
[4]V. G. Veselago, Sov. Phys. Usp. **10**, 509 (1968).
[5]D. R. Smith and N. Kroll, Phys. Rev. Lett. **85**, 2933 (2000).
[6]G. V. Eleftheriades and K. G. Balmain, *Negative-Refraction Metamaterials: Fundamental Principles and Applications* (Wiley, New York, 2005).
[7]H. N. S. Krishnamoorthy, Z. Jacob, E. Narimanov, I. Kretzschmar, and V. M. Menon, Science **336**, 205 (2012).
[8]C. L. Cortes, W. Newman, S. Molesky, and Z. Jacob, J. Opt. **14**, 063001 (2012).
[9]O. Kidwai, S. V. Zhukovsky, and J. E. Sipe, Opt. Lett. **36**, 2530 (2011).
[10]A. N. Poddubny, P. A. Belov, and Yu. S. Kivshar, Phys. Rev. A **84**, 023807 (2011).
[11]I. Iorsh, A. Poddubny, A. Orlov, P. Belov, and Yu. S. Kivshar, Phys. Lett. A **376**, 185 (2012).
[12]Z. Jacob and V. M. Shalaev, Science **334**, 463 (2011).
[13]R. K. Fisher and R. W. Gould, Phys. Rev. Lett. **22**, 1093 (1969).
[14]K. G. Balmain, A. A. E. Luttegen, and P. C. Kremer, IEEE Antennas Propag. Lett. **1**, 146 (2002).
[15]K. G. Balmain, A. A. E. Luettgen, and P. C. Kremer, IEEE Trans. Antennas. Propag. **51**, 2612 (2003).
[16]G. V. Eleftheriades and O. F. Siddiqui, IEEE Trans. Microwave Theory Technol. **53**, 396 (2005).
[17]O. F. Siddiqui and G. V. Eleftheriades, J. Franklin Inst. **348**, 1285 (2011).
[18]C. Caloz and T. Itoh, *Electromagnetic Materials* (Wiley, 2005).
[19]A. Grbic and G. V. Eleftheriades, IEEE Trans. Antennas Propag. **51**, 2604 (2003).
[20]A. Grbic and G. V. Eleftheriades, J. Appl. Phys. **98**, 043106 (2005).
[21]P. Alitalo, S. Maslovski, and S. Tretyakov, J. Appl. Phys. **99**, 124910 (2006).
[22]P. Alitalo, S. Maslovski, and S. Tretyakov, J. Appl. Phys. **99**, 064912 (2006).
[23]G. Gok and A. Grbic, IEEE Trans. Antennas Propag. **58**, 1559 (2010).
[24]C. F. M. Carobbi, L. M. Millanta, and L. Chiosi, IEEE International Symposium on Electromagnetic Compatibility **1**, 35 (2000).